THE JOURNAL OF PHYSICAL CHEMISTRY C

Article

Cite This: J. Phys. Chem. C 2019, 123, 25128−25134

pubs.acs.org/JPCC

Chemical Dissolution of Pt(111) during Potential Cycling under Negative pH Conditions Studied by Operando X-ray Photoelectron Spectroscopy

Harri Ali-Löytty,*[,†,‡] Markku Hannula,[†] Mika Valden,[†] André Eilert,[‡] Hirohito Ogasawara,[§] and Anders Nilsson[‡,∥]

[†]Surface Science Group, Photonics Laboratory, Tampere University, FI-33014 Tampere, Finland

[‡]SUNCAT Center for Interface Science and Catalysis and [§]Stanford Synchrotron Radiation Light Source (SSRL), SLAC National Accelerator Laboratory, 2575 Sand Hill Road, Menlo Park, California 94025, United States

[∥]Department of Physics, Stockholm University, Fysikum, 106 91 Stockholm, Sweden

Supporting Information

ABSTRACT: Dissolution of a platinum catalyst is a major degradation mechanism of fuel cells, but the exact reaction mechanism has remained unclear. Here, electrochemical ambient pressure X-ray photoelectron spectroscopy (EC-APXPS) was utilized to provide direct information on chemical species on a single-crystal Pt(111) electrode under extremely low pH conditions. Measurements were conducted using a novel condensed electrolyte film electrochemical cell applying work function measurement as a loss-free probe for electrochemical potential. We show that platinum can dissolve chemically as Pt^{2+} ion during potential cycling and redeposit as Pt^{2+} at the onset potential for cathodic reactions. The dissolution of Pt does not require electrochemical oxidation via oxide place exchange. In contrast, the adsorption of oxygenated species (OH* or O*) at the onset potential for anodic reactions is a sufficient prerequisite to the dissolution. These results provide new insight into the degradation mechanism of Pt under extremely low pH conditions, predicted by the Pourbaix diagram, having practical applications to the durability of Pt-based catalysts in electrochemical energy conversion devices.

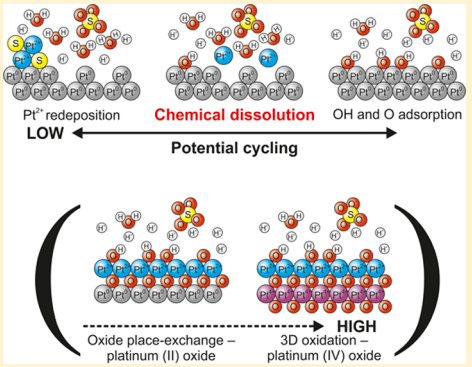

INTRODUCTION

Platinum-based catalysts are the most active electrocatalysts for electrochemical energy conversion devices such as electrolyzers and fuel cells.[1] Despite being one of the most resistive metals to corrosion, degradation of Pt catalyst has been identified as one of the key issues limiting the long-term durability of proton exchange membrane fuel cells (PEMFs). Out of the three degradation modes of a PEMF stack (load cycling, idling, and start/stop cycles), degradation during start/stop cycles is the largest.[2,3] Likewise, Pt dissolution is the strongest during potential cycling, which occurs during the start-up and shutdown of a fuel cell.[4] The Pourbaix diagram[5] predicts Pt corrosion in a narrow potential range close to 1.0 V only for pH < 0, which is, however, outside the ideal working environment of a PEMF cathode.[6] Therefore, the investigations of Pt corrosion under nonideal conditions are likely to provide new insights to the Pt dissolution mechanism and following Pt redeposition at PEMF cathodes. For example, the results obtained for model catalytic systems under potential cycling conditions in dilute acids, as summarized below, have contributed significantly to our current understanding of Pt dissolution mechanism. In contrast, extremely low pH conditions have been rarely addressed, albeit any diffusion problem within the porous cathode induces concentration gradients[7] that might result in a decrease in the local pH value, possibly even below 0.

Pt dissolution is a transient process, and the dissolution rate during cathodic polarization is more significant than during anodic polarization.[8] The common understanding is that oxygenated Pt species that form at high anodic potentials contribute to the dissolution mechanism. However, in the lack of a direct chemical probe, the exact type and role of these species have remained controversial and several dissolution mechanisms have been proposed, as summarized recently by Myers et al. in ref 9. One of the disagreements is the role of Pt oxidation on dissolution. The initial steps of electrochemical Pt oxidation include adsorption of OH or O.[10,11] Then, the oxidation onsets via place-exchange reaction between the adsorbed oxygenated species (OH* or O*) and surface Pt^0 resulting in the formation of a two-dimensional PtO (platinum(II) oxide) or $Pt(OH)_2$ (platinum(II) hydroxide) layer with subsurface oxygen atoms. With increasing anodic potential, oxidation proceeds to three-dimensional film growth and eventually to the formation of PtO_2 (platinum(IV) oxide).

Received: May 31, 2019
Revised: September 24, 2019
Published: September 25, 2019

DOI: 10.1021/acs.jpcc.9b05201
J. Phys. Chem. C 2019, 123, 25128−25134

When potential is then decreased, the Pt oxides are electrochemically reduced.

Since XPS analysis became feasible at high enough pressure for H_2O condensation, electrochemical devices allowing XPS analysis of electrodes under aqueous electrochemical conditions have been developed.[12−15] The ongoing development work is aiming at the analysis of reaction intermediate species on well-defined model catalytic systems during an electrocatalytic reaction, i.e., operando. Such information would provide critically needed input to the development of superior catalyst materials for (photo)electrochemical energy conversion devices.[16] However, the desire for high surface sensitivity sets challenges to the electrochemical cell design. Performance of XPS in the analysis of electrochemical devices has been demonstrated on a device based on a proton exchange membrane[17] and on a conventional electrochemical cell using the "dip & pull" approach.[14] The conductive membrane provides low ohmic resistance between the electrodes but the approach is only suitable to the analysis of nanoparticles. The performance of the membrane cell can be improved by an additional graphene capping layer that confines a liquid electrolyte thin film between the nanoparticles and the vacuum of the XPS chamber.[18] On the other hand, the dip & pull approach allows the use of planar electrodes, but the charge is transferred through a thin electrolyte film with high ohmic resistance that limits the operando analysis to low current densities.[19]

In this work, we use synchrotron light-mediated soft X-ray ambient pressure X-ray photoelectron spectroscopy (APXPS)[17] together with a novel condensed electrolyte film electrochemical cell depicted in Figure 1 to probe chemical species on a single-crystal Pt(111) electrode surface under acidic electrochemical conditions (Supporting Information). We show that potential cycling within low current region induces dissolution of Pt that adsorbs at the onset of cathodic reactions as $Pt^{2+}(-S)$. At the onset of anodic reactions, only adsorbed oxygenated species (OH* or O*) on the surface are detected, which indicates that the oxidation of Pt via place-exchange reaction is not a prerequisite to the dissolution.

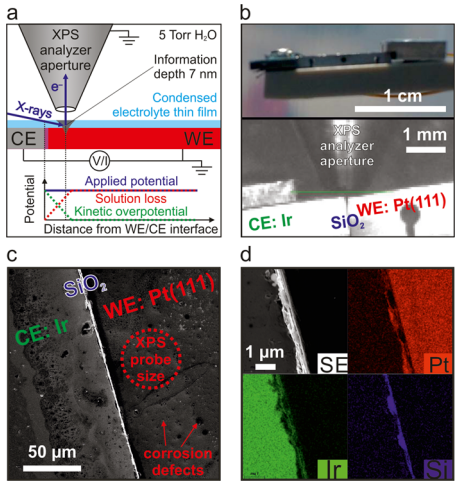

Figure 1. Condensed electrolyte film electrochemical cell applied in the operando EC-APXPS analysis of Pt dissolution. (a) Schematic representation of the experimental setup and (b) pictures of the electrochemical cell: the Pt(111) working electrode (WE) is electrically isolated from the Ir counter electrode (CE) by a SiO_2 film and the electrolyte adlayer is formed via rehydration of H_2SO_4 deposited ex situ onto the electrode surface by adjusting the relative humidity below 100%. (c) SEM and (d) EDS images of the CE/WE interface measured after EC-APXPS experiments revealing degradation of Pt(111) surface during the experiments.

EXPERIMENTAL METHODS

Condensed Electrolyte Film Electrochemical Cell. The Pt(111) single crystal employed in the experiments as the working electrode (WE) was manufactured by Surface Preparation Laboratory B.V. (Netherlands). The (111)-oriented top surface of a 10 mm × 6.6 mm × 1 mm crystal was aligned to <0.5 degree, and both the top surface and one of the 6.6 mm × 1 mm side surfaces were polished to <0.03 μm roughness. The Ir counter electrode (CE) was prepared on a piece of polycrystalline Ta (10 mm × 5 mm × 1 mm) by the evaporation of the Ti (10 nm) wetting layer followed by the evaporation of Ir (300 nm) on the top surface and sputter deposition of SiO_2 (500 nm) on one of the 10 mm × 1 mm side surfaces. Prior to the thin film growth, the top and side surfaces were polished to mirror finish.

The electrochemical cell was assembled on a polyether-etherketone (PEEK) polymer framework that was designed to couple the electrode pieces mechanically side by side. In the assembled electrochemical cell, the SiO_2 layer serves as electrical insulation between the WE and CE. Before the cell assembly, the Pt(111) WE was flame-annealed at white heat for 3 min using a butane torch, and while still orange-yellow, the WE was transferred into a flask through which inert N_2 (99.999%) cooling gas was flowing until the room temperature was reached in 2 min.[20] Cooling of Pt(111) after flame-annealing in either H_2 or N_2 has been shown to result in well-ordered and flat surface.[20]

After the cell assembly, the H_2SO_4 electrolyte layer was prepared by depositing a droplet of 1 M H_2SO_4 solution ex situ onto the electrode surface. Then, the electrochemical cell was introduced into the APXPS vacuum chamber where the surface was rehydrated by exposing it to H_2O vapor at room temperature.[21] The thickness of the electrolyte layer was controlled by adjusting the H_2O pressure in the measurement chamber below the condensation limit by backfilling the chamber with Milli-Q H_2O using a leak valve. The Milli-Q H_2O was degassed by multiple freeze−pump−thaw cycles before introduction into the measurement chamber. Eventually, the rehydration of vacuum-dehydrated H_2SO_4 solution created an electrolyte adlayer for the EC-APXPS measurements with concentration corresponding to saturated 18.8 M H_2SO_4 solution.[22] The concentration of the electrolyte adlayer was approximated based on measured XPS signals of S 2p and O 1s (Supporting Information). The pH of the condensed H_2SO_4 electrolyte film was assumed to be negative.[23] During the EC-APXPS measurements, the pH_2O was fixed at 5 Torr, which was found to provide sufficient ionic conductivity between the electrodes, as shown in Figure S1. Based on the attenuation of the Pt 4f XPS signal, the thickness of the electrolyte layer during EC-APXPS measurements presented in Figure 3 was estimated to be 4−10 nm. After the experiments, the Pt(111)-WE|SiO_2(0.5 μm)|Ir-CE electrode assembly was analyzed by scanning electron microscopy (SEM) and energy-dispersive X-ray spectroscopy (EDS).

APXPS Measurements. XPS measurements were performed using the APXPS system on beamline 13−2 at the Stanford Synchrotron Radiation Lightsource.[24] The electrochemical cell assembly was inserted into the gas cell of the

DOI: 10.1021/acs.jpcc.9b05201
J. Phys. Chem. C 2019, 123, 25128−25134

APXPS system where the sample alignment and navigation on the electrode surface were performed at 0.2 μm steps through piezoelectric positioners (Attocube, Germany). During the EC-APXPS measurements, the sample was positioned approximately 50 μm away from the spectrometer entrance cone with 50 μm diameter. To minimize the ohmic losses within the thin electrolyte film,[19] all EC-APXPS data were collected within 100 μm distance from the WE−CE interface. To mitigate possible X-ray beam damage to the surface, the X-ray spot (50 × 10 μm^2, the incidence angle of 4°) was moved on the sample between the experiments. No signs of beam damage were observed in the SEM analysis after the experiments. Therefore, the inhomogeneous surface compositions observed in the XPS and SEM analyses were not the signs of beam damage but attributed to the preparation of the electrolyte film.

During the electrochemical measurements, the current−voltage characteristics were recorded in a two-electrode configuration with a potentiostat (BioLogic, France). All measurements were conducted at room temperature. It is worth noting that the electrochemical potential of a thin electrolyte film electrochemical cell is not necessarily homogeneous over the electrode surface.[19] Therefore, the incorporation of a conventional reference electrode was omitted and the changes in the local electrochemical potential with applied bias potential were monitored through the changes in the local work function.

A shift in the XPS position of gas and liquid-phase species with applied potential corresponds to a change in the local work function, i.e., solution loss-free electrochemical potential at a position where XPS data is collected (cf. a reference electrode with a Luggin capillary). Because of ohmic solution losses, the peak shifts begin to deviate from 1:1 relationship with applied potential when current increases. Consequently, a conventional reference electrode outside the XPS position would not provide accurate electrochemical potential at the XPS position as we showed in ref 19, and the CV characteristics outside the linear range do not present the charge-transfer properties at the XPS position. Thus, clearly distinct XPS peak of gas-phase H_2O was utilized here to monitor the electrochemical potential. For example, with +1.6 V applied potential, the solution loss-free potential at the XPS position, i.e., the O 1s $H_2O(g)$ peak shifts from 0 V, was +1.15 V. Likewise, for the applied potential of −0.9 V, the solution loss-free potential at the XPS position was −0.53 V. Because of the inherent limitation of the thin electrolyte film to low reaction current, the potential at the XPS position maintained between the onset potentials for cathodic and anodic reactions during the course of experiments.

The photoemission signal was recorded using a differentially pumped customized VG Scienta SES 100 electron spectrometer. The working electrode was grounded to the spectrometer, and the XPS binding energy scale was referenced to the Fermi level set to 0 eV. All of the spectra were recorded at 688 eV photon energy. The information depths (3 × inelastic mean free path) of Pt 4f and O 1s photoelectrons with corresponding kinetic energies were 7.1 and 2.9 nm in liquid H_2O, respectively.[25] The chemical states of elements were determined from XPS spectra by least-squares fitting of Gaussian−Lorentzian (GL) lineshapes to the photoelectron peaks after subtracting a Shirley background. To account for the asymmetry of Pt 4f peaks, the GL lineshape was modified by the exponential blend. The analysis was carried out using the CasaXPS software (version 2.3.18).[26]

RESULTS AND DISCUSSION

Due to the inherent limitation of thin electrolyte film electrochemical cells to low reaction current,[19] the operando EC-APXPS analysis is best suited to study phenomena that do not require charge transfer such as adsorption/desorption and dissolution. To mitigate the ohmic solution losses induced by the ultrathin (4−10 nm) condensed electrolyte film, XPS data were collected within 100 μm distance from the WE/CE interface. Figure 2 presents XPS peak shifts (Figure S3) as a function of applied potential together with a cyclic voltammogram (CV). Because of ohmic solution losses, the XPS peak shifts begin to deviate from 1:1 relationship with applied potential when current increases.[19] No sharp adsorption/desorption peaks of SO_4 or H were observed in the CV that are well characterized for defect-free Pt(111) surface in dilute H_2SO_4.[11] Instead, the broad anodic and cathodic waves between −0.5 and +1.0 V are similar to the ones observed by Kodera et al. in ref 27 on Pt in concentrated H_2SO_4. Kodera et al. reported that H adsorption/desorption peaks completely disappeared in concentrated H_2SO_4 and assigned the broad anodic and cathodic waves to Pt corrosion. Furthermore, compared to dilute H_2SO_4, significantly higher Pt dissolution rate is expected under concentrated H_2SO_4.[8] The anodic peak at +1.3 V is assigned to Pt oxidation that precedes the oxygen evolution for potentials > +1.6 V.[28] Hydrogen evolution was observed for potentials < −1.5 V (Figure S1).

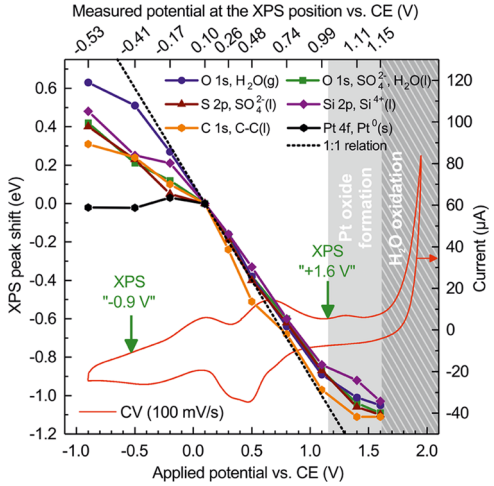

Figure 2. XPS peak shifts vs applied potential overlaid with cyclic voltammogram (CV). XPS data was collected on Pt(111)-WE close to the WE/CE interface during potentiostatic measurement from −0.9 to +1.6 V for Pt(111)-WE|SiO_2(0.5 μm)|Ir-CE electrode assembly with H_2SO_4 electrolyte adlayer. The CV was recorded between the WE and CE. The IV characteristics are dominated by the electrode areas closest to the WE/CE interface where the ohmic solution losses are the lowest. In contrast, the solution loss-free potentials at the XPS position for the applied potentials of −0.9 and +1.6 V are depicted with green arrows. Pt 4f was not detected in the experiment for potentials > +0.1 eV due to the build-up of contamination during prolonged data acquisition (Supporting Information).

Figure 3 shows XP spectra of Pt 4f and O 1s regions during an experimental run. First, Pt(111)-WE was flame-annealed ex situ and the surface was confirmed to be free from Pt oxides as

DOI: 10.1021/acs.jpcc.9b05201
J. Phys. Chem. C 2019, 123, 25128−25134

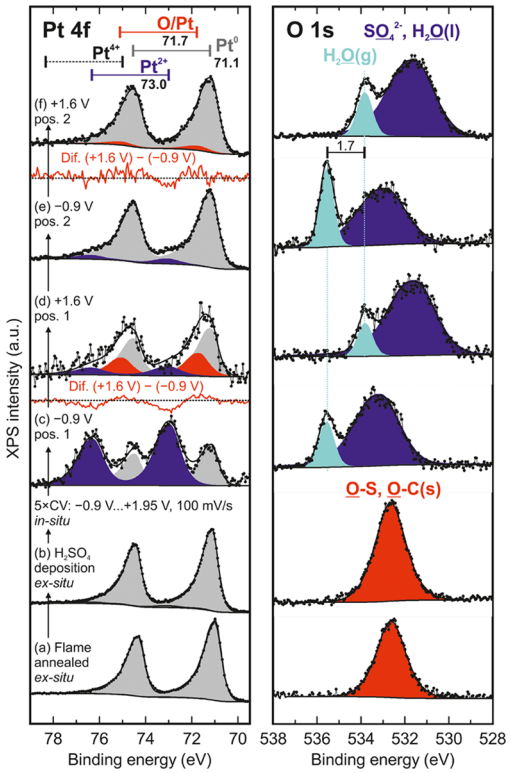

Figure 3. XP spectra of Pt 4f and O 1s regions excited with 688 eV photons during an experimental run on Pt(111)-WE|SiO_2(0.5 μm)|Ir-CE electrode assembly. The spectra were first recorded (a) after ex situ flame-annealing and (b) after ex situ deposition of H_2SO_4. Then, the electrode assembly was rehydrated in situ and subjected to 5 potential scans between −0.9 and +1.95 V. (c−f) After the CVs XP spectra were recorded at the applied potentials of −0.9 V and at +1.6 V (at the measured potentials of −0.53 and +1.15 V, respectively) for two different locations close to the WE/CE interface. The Pt 4f difference spectra in red depict the similar change induced by the potential step for both locations.

evidenced by a single Pt 4f doublet with Pt $4f_{7/2}$ at 71.1 eV corresponding to metallic Pt (Figure 3a). The O 1s peak at 532.5 eV was assigned to adventitious contamination during the sample transfer.[29] The Pt(111)-WE remained oxide free also after the ex situ deposition of H_2SO_4 on electrodes (Figure 3b). The vacuum-dehydrated H_2SO_4 on the sample has similar O 1s binding energy with the adventitious contamination, and, therefore, only one component was fitted to O 1s.[30] Then, the vacuum-dehydrated H_2SO_4 was rehydrated in situ, and the electrode assembly was subjected 5 potential cycles between −0.9 and +1.95 V at 100 mV/s (between −0.53 and +1.15 V at the XPS position) that induced the degradation of Pt(111) surface. Thus, this potential cycling treatment in concentrated H_2SO_4 between the onset of anodic and cathodic reactions can be considered as an accelerated corrosion test. Because of the build-up of adventitious C- and Si-based contamination during prolonged data acquisition, the operando EC-APXPS measurements were carefully planned and focused only on the Pt species at two potentials. Based on the XPS peak shifts response to applied potential during potentiostatic measurement, all of the Si and most of the C species were able to be assigned to dissolved impurities in the electrolyte film (Supporting Information) that were, therefore, assumed to have a little effect on the Pt dissolution mechanism.

After the electrochemical cycling between −0.9 and +1.6 V, O 1s and Pt 4f spectra were recorded at −0.9 V at a location close to the WE/CE interface (Figure 3c) and immediately after, Pt 4f and O 1s, in this order, were recorded at +1.6 V at the same location (Figure 3d). After the data acquisition at the first location, the measurement was repeated at another location also close to the WE/CE interface (Figure 3e,f). The current−voltage characteristics during the CVs and in situ XPS measurement are presented in Figure S4.

The O 1s spectra recorded under electrochemical conditions (Figure 3c−f) consist of two clearly distinct peaks that both shift with the applied potential. The narrow gas-phase H_2O peak at the high binding energy side shifts −1.7 eV (in binding energy) when the applied potential is changed from −0.9 to +1.6 V. Similar peak positions and shifts were observed for both XPS locations, which indicate that the electrochemical potentials at both XPS locations were similar. The broad O 1s peak at the low binding energy side was dominated by the liquid-phase species assignable to H_2O and SO_4^{2-}.[30] We note that adsorbed oxygenated species (e.g., −OH, −O, and $-H_2O$)[12] were hard to distinguish from the broad O 1s peak due to the low information depth (ID = 2.9 nm). In particular, the broad peak at +1.6 V extends to the binding energy range of oxygenated Pt, which appears between 529.7 eV[28,31] (Pt−O*), 530.1 eV (PtO_2),[31] and 530.5 eV (Pt−OH*).[28] Thus, more bulk sensitive Pt 4f signal (ID = 7.1 nm) provided here a better probe for the adsorbed surface species without the interference from different oxygenated species from liquid and solid phases that have similar binding energies in O 1s.

The fitting of Pt 4f spectra recorded under electrochemical conditions (Figure 3c−f) required two more doublets in addition to the metallic Pt. The Pt 4f difference spectra depicted as red lines in Figure 3 show an increase in intensity at 71.7 eV and concurrent decrease at 73.0 eV (and at corresponding energies of Pt $4f_{5/2}$) when the potential is changed from −0.9 to +1.6 V. The same change was observed for both XPS locations, albeit with different intensity ratio with respect to Pt^0. These new peaks were assigned according to their binding energies to adsorbed oxygen species (OH* or O*) on Pt (O/Pt) and Pt^{2+}, respectively.[31−33]

Besides the chemisorbed oxygen species reported in the literature for Pt electrodes,[32] the binding energy of O/Pt component corresponds to the 1 ML surface oxide on Pt(111) that was observed under oxygen ambient at elevated temperatures before the 3D oxide growth.[31] Compared to the lattice restructuring involved with the oxide place exchange,[34] the formation of 1 ML surface oxide does not involve subsurface oxygen, and, therefore, it is not considered here as the oxide place-exchange reaction. However, the 1 ML surface-oxide formation involves lifting of Pt atoms, i.e., place change, that can induce strong modification to the Pt−O bonding at the surface compared to chemisorbed oxygen species alone. In other words, Miller et al. showed that restructuring of Pt(111) surface does not require oxide place exchange.[31] Thus, it is suggested that Pt place change, an initial stage of oxide place exchange, is a sufficient prerequisite to the Pt dissolution. This result does not contradict with the previous understanding that the degree of Pt surface restructuring during potential cycling is directly proportional to the dissolution rate[8] but reveals that oxide place exchange is not necessary. The difference in the Pt 4f spectrum between the two XPS locations is an indication of inhomogeneous surface composition that is likely a result of nonuniform

DOI: 10.1021/acs.jpcc.9b05201
J. Phys. Chem. C 2019, 123, 25128−25134

dehydration of H_2SO_4 solution during the preparation of the electrolyte film. The inhomogeneous surface composition is also evident from the SEM image measured after the experiment (Figure 1c) that shows localized corrosion defects.

The adsorption of oxygenated species as the potential is increased is generally accepted as the initial reaction step of electrochemical oxidation. In contrast, the behavior of Pt^{2+} seems at first contradictory as the electrochemical reduction reaction is expected with decreasing potential. However, similar to oxidation, reduction would require charge transfer, which is strongly limited by the thin electrolyte film. Therefore, we assign Pt^{2+} species at −0.9 V as redeposited Pt species that were dissolved during the potential cycling and migrated on the surface. The potential step from −0.9 to +1.6 V is suggested to induce migration of Pt^{2+} species to electrochemically inactive areas outside the XPS spot. We note that the XPS peak of dissolved Pt^{2+} species would have shifted −1.7 eV with the potential step, which contradicts the observed peak separation of 1.3 eV between the Pt^{2+} and O/Pt peaks. In fact, the formation of Pt^{2+}−S species was observed by Kodera et al. in concentrated H_2SO_4.[27] In PEMF, dissolved Pt has been proposed to redeposit at electrochemically inactive areas,[27] which is supported by the EDS maps in Figure 1d that show some Pt on the SiO_2 insulator between the WE and CE. We emphasize that the electrochemical oxidation of Pt via oxide place exchange induced by the anodic potential step would appear as an increase in Pt^{2+} and further 3D oxide layer growth as an increase in Pt^{4+} (reported Pt $4f_{7/2}$ values range from 73.4 eV[18] to 75.0 eV[32]) with corresponding changes in O 1s either of which were not observed.

The presented results focus on the identification of surface species related to the dissolution mechanism on a model Pt electrode by operando EC-APXPS. It is noted that the experimental conditions were drastically different from the ideal operation environment of a PEMF and from typical test conditions applied to study electrocatalyst materials in terms of mass transfer and electrolyte concentration. Therefore, comparison between the results obtained using the condensed electrolyte film cell with severe mass transfer limitation and results obtained using the conventional electrochemical cell with low solution resistance should be made with caution. However, the concentration of the condensed H_2SO_4 electrolyte film is extremely high corresponding to pH where corrosion of Pt has been predicted by the Pourbaix diagram (pH < 0).[5] Thus, the results provide insights to the Pt corrosion mechanism at extremely low pH, where the mechanism might differ from that in dilute H_2SO_4.

CONCLUSIONS

In conclusion, our operando EC-APXPS results provide direct information on chemical species involved in Pt dissolution under negative pH conditions. Measurements were conducted using a novel condensed electrolyte film electrochemical cell applying work function measurement as a loss-free probe for electrochemical potential. The results support chemical dissolution during potential cycling without charge transfer between the electrodes via $Pt{-}(OH^*)_2 + 2H^+ \rightarrow Pt^{2+} + 2H_2O$ (or $Pt{-}O^* + 2H^+ \rightarrow Pt^{2+} + H_2O$) and redeposition of Pt^{2+} ions at low potentials.[35] In other words, Pt dissolution does not require electrochemical oxidation of Pt via oxide place exchange that has been the generally accepted reaction mechanism.[18,36] These results suggest that Pt place change, an initial stage of oxide place exchange, could follow the adsorption of oxygenated species and be a sufficient prerequisite to the Pt dissolution. This is deemed an important improvement to previous models that, because of the nonavailability of exacting surface spectroscopic methods, could not detect chemical dissolution of either elemental or oxidized Pt.[9] Therefore, these results provide new insight to the degradation mechanism of Pt under extremely low pH conditions, predicted by the Pourbaix diagram, which are far from ideal working environment of any electrochemical energy conversion devices such as PEMF but might exist under condition where diffusion of reactants is severely limited.

ASSOCIATED CONTENT

Supporting Information

The Supporting Information is available free of charge on the ACS Publications website at DOI: 10.1021/acs.jpcc.9b05201.

Details on the performance of the condensed electrolyte film electrochemical cell at APXPS beamline 13−2 at SSRL, XPS data collected during potentiostatic measurement from −0.9 to +1.6 V, current−voltage characteristics during operando EC-APXPS measurements, determination of the electrolyte concentration from XPS data (PDF)

AUTHOR INFORMATION

Corresponding Author

*E-mail: Harri.Ali-Loytty@tuni.fi.

ORCID

Markku Hannula: 0000-0003-1110-7439
Hirohito Ogasawara: 0000-0001-5338-1079
Anders Nilsson: 0000-0003-1968-8696

Author Contributions

The manuscript was written through contributions of all of the authors. All of the authors have given approval to the final version of the manuscript.

Notes

The authors declare no competing financial interest.

ACKNOWLEDGMENTS

We acknowledge Daniel Friebel, May Ling Ng, Sloan Roberts, Jeffrey Beeman, Ian D. Sharp, and Mike Swansson for the assistance, discussions, and co-operation during the project. This material is based upon the work performed by the Joint Center for Artificial Photosynthesis, a DOE Energy Innovation Hub, supported through the Office of Science of the U.S. Department of Energy under Award Number DE-SC0004993. Use of the Stanford Synchrotron Radiation Lightsource, SLAC National Accelerator Laboratory, is supported by the U.S. Department of Energy, Office of Science, Office of Basic Energy Sciences under Contract No. DE-AC02-76SF00515. This work is a part of the Academy of Finland Flagship Programme, Photonics Research and Innovation (PREIN) (Decision No. 320165). This work was supported by Jane & Aatos Erkko Foundation and the Academy of Finland (Grant Nos. 309920, 326461, 286713, 326406, 310359). H.A.-L. was supported by the Finnish Cultural Foundation, KAUTE Foundation, and Jenny and Antti Wihuri Foundation. M.H. was supported by the Graduate School of Tampere University of Technology.

DOI: 10.1021/acs.jpcc.9b05201
J. Phys. Chem. C 2019, 123, 25128−25134

REFERENCES

(1) Katsounaros, I.; Cherevko, S.; Zeradjanin, A. R.; Mayrhofer, K. J. J. Oxygen Electrochemistry as a Cornerstone for Sustainable Energy Conversion. *Angew. Chem., Int. Ed.* **2014**, *53*, 102−121.

(2) Mench, M. M.; Kumbur, E. C.; Veziroglu, T. N. *Polymer Electrolyte Fuel Cell Degradation*; Elsevier Science: Saint Louis, 2011.

(3) Cherevko, S.; Keeley, G. P.; Geiger, S.; Zeradjanin, A. R.; Hodnik, N.; Kulyk, N.; Mayrhofer, K. J. J. Dissolution of Platinum in the Operational Range of Fuel Cells. *ChemElectroChem* **2015**, *2*, 1471−1478.

(4) Topalov, A. A.; Katsounaros, I.; Auinger, M.; Cherevko, S.; Meier, J. C.; Klemm, S. O.; Mayrhofer, K. J. J. Dissolution of Platinum: Limits for the Deployment of Electrochemical Energy Conversion? *Angew. Chem., Int. Ed.* **2012**, *51*, 12613−12615.

(5) Pourbaix, M. *Atlas of Electrochemical Equilibria in Aqueous Solutions, Second English Edition*; National Association of Corrosion: Houston, TX, 1974.

(6) Guilminot, E.; Corcella, A.; Charlot, F.; Maillard, F.; Chatenet, M. Detection of Pt z + Ions and Pt Nanoparticles Inside the Membrane of a Used PEMFC. *J. Electrochem. Soc.* **2007**, *154*, B96−B105.

(7) Park, Y.-C.; Tokiwa, H.; Kakinuma, K.; Watanabe, M.; Uchida, M. Effects of Carbon Supports on Pt Distribution, Ionomer Coverage and Cathode Performance for Polymer Electrolyte Fuel Cells. *J. Power Sources* **2016**, *315*, 179−191.

(8) Topalov, A. A.; Cherevko, S.; Zeradjanin, A. R.; Meier, J. C.; Katsounaros, I.; Mayrhofer, K. J. J. Towards a Comprehensive Understanding of Platinum Dissolution in Acidic Media. *Chem. Sci.* **2014**, *5*, 631−638.

(9) Myers, D. J.; Wang, X.; Smith, M. C.; More, K. L. Potentiostatic and Potential Cycling Dissolution of Polycrystalline Platinum and Platinum Nano-Particle Fuel Cell Catalysts. *J. Electrochem. Soc.* **2018**, *165*, F3178−F3190.

(10) Conway, B. E. Electrochemical Oxide Film Formation at Noble Metals as a Surface-Chemical Process. *Prog. Surf. Sci.* **1995**, *49*, 331−452.

(11) Marković, N. M.; Ross, P. N., Jr. Surface Science Studies of Model Fuel Cell Electrocatalysts. *Surf. Sci. Rep.* **2002**, *45*, 117−229.

(12) Casalongue, H. S.; Kaya, S.; Viswanathan, V.; Miller, D. J.; Friebel, D.; Hansen, H. A.; Nørskov, J. K.; Nilsson, A.; Ogasawara, H. Direct Observation of the Oxygenated Species during Oxygen Reduction on a Platinum Fuel Cell Cathode. *Nat. Commun.* **2013**, *4*, No. 2817.

(13) Velasco-Velez, J. J.; Pfeifer, V.; Hävecker, M.; Weatherup, R. S.; Arrigo, R.; Chuang, C.-H.; Stotz, E.; Weinberg, G.; Salmeron, M.; Schlögl, R.; et al. Photoelectron Spectroscopy at the Graphene−Liquid Interface Reveals the Electronic Structure of an Electrodeposited Cobalt/Graphene Electrocatalyst. *Angew. Chem., Int. Ed.* **2015**, *54*, 14554−14558.

(14) Axnanda, S.; Crumlin, E. J.; Mao, B.; Rani, S.; Chang, R.; Karlsson, P. G.; Edwards, M. O. M.; Lundqvist, M.; Moberg, R.; Ross, P.; et al. Using "Tender" X-Ray Ambient Pressure X-Ray Photoelectron Spectroscopy as A Direct Probe of Solid-Liquid Interface. *Sci. Rep.* **2015**, *5*, No. 9788.

(15) Karslıoğlu, O.; Nemsak, S.; Zegkinoglou, I.; Shavorskiy, A.; Hartl, M.; Salmassi, F.; Gullikson, E.; Ng, M.-L.; Rameshan, C.; Rude, B.; et al. Aqueous Solution/Metal Interfaces Investigated in Operando by Photoelectron Spectroscopy. *Faraday Discuss.* **2015**, *180*, 35−53.

(16) Soriaga, M. P.; Baricuatro, J. H.; Javier, A. C.; Kim, Y.-G.; Cummins, K. D.; Tsang, C. F.; Hemminger, J. C.; Bui, N. N.; Stickney, J. L. Electrochemical Surface Science of CO2 Reduction at Well-Defined Cu Electrodes: Surface Characterization by Emersion, Ex Situ, In Situ, and Operando Methods. In *Reference Module in Chemistry, Molecular Sciences and Chemical Engineering*; Elsevier, 2018; pp 562−576.

(17) Ogasawara, H.; Kaya, S.; Nilsson, A. Operando X-Ray Photoelectron Spectroscopy Studies of Aqueous Electrocatalytic Systems. *Top. Catal.* **2016**, *59*, 439−447.

(18) Mom, R.; Frevel, L.; Velasco-Vélez, J.-J.; Plodinec, M.; Knop-Gericke, A.; Schlögl, R. The Oxidation of Platinum under Wet Conditions Observed by Electrochemical X-Ray Photoelectron Spectroscopy. *J. Am. Chem. Soc.* **2019**, *141*, 6537−6544.

(19) Ali-Löytty, H.; Louie, M. W.; Singh, M. R.; Li, L.; Sanchez Casalongue, H. G.; Ogasawara, H.; Crumlin, E. J.; Liu, Z.; Bell, A. T.; Nilsson, A.; et al. Ambient-Pressure XPS Study of a Ni−Fe Electrocatalyst for the Oxygen Evolution Reaction. *J. Phys. Chem. C* **2016**, *120*, 2247−2253.

(20) Kibler, L. A.; Cuesta, A.; Kleinert, M.; Kolb, D. M. In-Situ STM Characterisation of the Surface Morphology of Platinum Single Crystal Electrodes as a Function of Their Preparation. *J. Electroanal. Chem.* **2000**, *484*, 73−82.

(21) Nemšák, S.; Shavorskiy, A.; Karslioglu, O.; Zegkinoglou, I.; Rattanachata, A.; Conlon, C. S.; Keqi, A.; Greene, P. K.; Burks, E. C.; Salmassi, F.; et al. Concentration and Chemical-State Profiles at Heterogeneous Interfaces with Sub-Nm Accuracy from Standing-Wave Ambient-Pressure Photoemission. *Nat. Commun.* **2014**, *5*, No. 5441.

(22) Trotochaud, L.; Head, A. R.; Karslıoğlu, O.; Kyhl, L.; Bluhm, H. Ambient Pressure Photoelectron Spectroscopy: Practical Considerations and Experimental Frontiers. *J. Phys.: Condens. Matter* **2017**, *29*, No. 053002.

(23) Nordstrom, D. K.; Alpers, C. N.; Ptacek, C. J.; Blowes, D. W. Negative PH and Extremely Acidic Mine Waters from Iron Mountain, California. *Environ. Sci. Technol.* **2000**, *34*, 254−258.

(24) Kaya, S.; Ogasawara, H.; Näslund, L.-Å.; Forsell, J.-O.; Casalongue, H. S.; Miller, D. J.; Nilsson, A. Ambient-Pressure Photoelectron Spectroscopy for Heterogeneous Catalysis and Electrochemistry. *Catal. Today* **2013**, *205*, 101−105.

(25) Tanuma, S.; Powell, C. J.; Penn, D. R. Calculations of Electron Inelastic Mean Free Paths. V. Data for 14 Organic Compounds over the 50-2000 EV Range. *Surf. Interface Anal.* **1994**, *21*, 165−176.

(26) Fairley, N. *CasaXPS: Spectrum Processing Software for XPS, AES and SIMS*, Version 2.3.19PR1.0.; Casa Software Ltd.

(27) Kodera, F.; Kuwahara, Y.; Nakazawa, A.; Umeda, M. Electrochemical Corrosion of Platinum Electrode in Concentrated Sulfuric Acid. *J. Power Sources* **2007**, *172*, 698−703.

(28) Wakisaka, M.; Udagawa, Y.; Suzuki, H.; Uchida, H.; Watanabe, M. Structural Effects on the Surface Oxidation Processes at Pt Single-Crystal Electrodes Studied by X-Ray Photoelectron Spectroscopy. *Energy Environ. Sci.* **2011**, *4*, 1662−1666.

(29) Naumkin, A. V.; Kraut-Vass, A.; Powell, C. J. *NIST XPS Database 20*, 2008; Vol. Version 4.0 (Web Version).

(30) Polčik, M.; Wilde, L.; Haase, J.; Brena, B.; Comelli, G.; Paolucci, G. High-Resolution XPS and NEXAFS Study of SO2 Adsorption on Pt(111): Two Surface SO2 Species. *Surf. Sci.* **1997**, *381*, L568−L572.

(31) Miller, D. J.; Öberg, H.; Kaya, S.; Sanchez Casalongue, H.; Friebel, D.; Anniyev, T.; Ogasawara, H.; Bluhm, H.; Pettersson, L. G. M.; Nilsson, A. Oxidation of Pt(111) under Near-Ambient Conditions. *Phys. Rev. Lett.* **2011**, *107*, No. 195502.

(32) Saveleva, V. A.; Papaefthimiou, V.; Daletou, M. K.; Doh, W. H.; Ulhaq-Bouillet, C.; Diebold, M.; Zafeiratos, S.; Savinova, E. R. *Operando* Near Ambient Pressure XPS (NAP-XPS) Study of the Pt Electrochemical Oxidation in H_2O and H_2O/O_2 Ambients. *J. Phys. Chem. C* **2016**, *120*, 15930−15940.

(33) Arrigo, R.; Hävecker, M.; Schuster, M. E.; Ranjan, C.; Stotz, E.; Knop-Gericke, A.; Schlögl, R. In Situ Study of the Gas-Phase Electrolysis of Water on Platinum by NAP-XPS. *Angew. Chem., Int. Ed.* **2013**, *52*, 11660−11664.

(34) Drnec, J.; Ruge, M.; Reikowski, F.; Rahn, B.; Carlà, F.; Felici, R.; Stettner, J.; Magnussen, O. M.; Harrington, D. A. Initial Stages of Pt(111) Electrooxidation: Dynamic and Structural Studies by Surface X-Ray Diffraction. *Electrochim. Acta* **2017**, *224*, 220−227.

(35) Lopes, P. P.; Tripkovic, D.; Martins, P. F. B. D.; Strmcnik, D.; Ticianelli, E. A.; Stamenkovic, V. R.; Markovic, N. M. Dynamics of Electrochemical Pt Dissolution at Atomic and Molecular Levels. *J. Electroanal. Chem.* **2018**, *819*, 123−129.

DOI: 10.1021/acs.jpcc.9b05201
J. Phys. Chem. C 2019, 123, 25128−25134

(36) Ahluwalia, R. K.; Papadias, D. D.; Kariuki, N. N.; Peng, J.-K.; Wang, X.; Tsai, Y.; Graczyk, D. G.; Myers, D. J. Potential Dependence of Pt and Co Dissolution from Platinum-Cobalt Alloy PEFC Catalysts Using Time-Resolved Measurements. *J. Electrochem. Soc.* **2018**, *165*, F3024−F3035.

DOI: 10.1021/acs.jpcc.9b05201
J. Phys. Chem. C 2019, 123, 25128−25134